LAWRENCE
LIVERMORE
NATIONAL
LABORATORY

UCRL-CONF-233635

Anodic Behavior of SAM2X5 Material Applied as Amorphous Coatings

Phillip D. Hailey, Joseph C. Farmer, Sumner D. Day, Raul B. Rebak

August 13, 2007

Materials Science and Technology 2007 (MS&T'07)
Detroit, MI, United States
September 16, 2007 through September 20, 2007

Disclaimer

Crevice Corrosion Susceptibility of Thermal Spray Coatings Using Electrochemical Techniques

P. D. Hailey, J. C. Farmer, S. D. Day and Raul B. Rebak
Lawrence Livermore National Laboratory
Livermore, California, USA

Keywords: Iron based amorphous alloys, SAM2X5, coatings, corrosion, S31600, N06022

Abstract

Iron-based amorphous alloys are desirable industrial materials since they are highly resistant to corrosion and possess enhanced hardness for wear resistance. The amorphous materials can be produced from the melt as powder and later spray deposited as coatings on large engineering structures. As a laboratory experiment, SAM2X5 powder was coated on electrochemical specimens of 304SS for testing. Results show that the coated specimens did not perform satisfactorily during the laboratory testing. This is because of partial devitrification during the deposition of the powder on the small specimen substrates.

Introduction

There has been a large industrial interest in amorphous metallic alloys due to their unique characteristics, including resistance to wear and superior corrosion resistance [1]. To produce an amorphous alloy from a liquid state, cooling rates in the order of 10^6 to 1 degrees Kelvin per second are required [1]. The addition of alloying elements may slow down the cooling requirements to produce amorphous materials. The amorphous alloys are chemically and structurally homogeneous since they do not contain grain boundaries, dislocations and secondary phases, which are common in the crystalline materials [1]. The corrosion resistance of amorphous alloys depends on the alloy composition [2-4]. Amorphous alloys may be more corrosion resistant than their polycrystalline cousins of equivalent composition. Amorphous alloys are hard and can be used in areas where both resistance to wear and corrosion are simultaneously needed. For example the typical Vickers hardness of the polycrystalline Alloy 22 (N06022) is 250 but the Vickers hardness of an amorphous material is higher than 1000 [5]. The fact that amorphous materials are highly corrosion resistant is generally attributed to the absence of crystalline defects in the alloy; however the actual mechanism of this resistance is still not fully understood [1]. When amorphous alloys partially or fully re-crystallize, they may lose some of their characteristic corrosion resistance. This process is called devitrification [6].

Iron based amorphous alloys are more economical to produce than the highly corrosion resistant nickel based alloys; therefore the use of amorphous materials seems attractive for economical reasons, besides their enhanced resistance to corrosion and desirable hardness [7].

Recently, Fe-based amorphous alloys have been produced in bulk compositions so they can be applied to the fabrication of many large structural components, including oceanic shipbuilding, nuclear, and oil and gas industries. These alloys are called bulk metallic glasses or structural amorphous metals (SAM) by DARPA (Defense Advanced Research Projects Agency). Fe is a desirable base element for alloys that may be used in large industrial applications not only because Fe is inexpensive but also because Fe-based bulk metallic glasses have a high glass forming ability, high mechanical properties and soft magnetic properties. [8] The newer Fe-based amorphous alloys can be produced at relatively slow cooling rates on the order of 100 Kelvin per second [9]. This allows the production of bulk amorphous metals tailored to specific applications using processes such as thermal spray. Fe-based amorphous alloys such as SAM2X5 may contain up to 15% (atomic) in boron (B), which make them attractive for nuclear applications as neutron absorbing structural material [10-11]. SAM2X5 is a candidate material for neutron absorption applications and a candidate to replace both borated stainless steels and recently developed nickel-chromium-molybdenum-gadolinium (Ni-Cr-Mo-Gd) alloys [12-13].

The aim of the current study was to evaluate the anodic behavior of SAM2X5 material applied as coatings on electrochemical specimens.

Experimental

Table 1 shows the nominal chemical composition of the studied alloys. The polycrystalline engineering alloys (316SS or S31600 and Alloy 22 or N06022) are reported only for comparative purposes. The amorphous alloy (SAM2X5) was deposited as a coating on a 304 stainless steel substrate. The amorphous alloy coating was deposited on a multiple crevice assembly (MCA) of lollipop type 304SS pre-cut specimen. Originally the SAM2X5 powder material was prepared at the NanoSteel company in Idaho Falls, ID. The powder was approximately 15 to 50 μm diameter particles (Figure 1) and it is identified as lot 06-015. The powder was later thermally sprayed on the polycrystalline 304SS substrate specimens at Plasma Technology Inc. in Torrance, CA. The thickness of the SAM2X5 coating on the electrochemical test specimens was approximately 0.015-inch (380-μm thick). The surface of the coated specimens looked sandy, uneven or rugose. X-ray studies have been conducted on the L9 coated MCA specimen showing basically an amorphous structure with some crystalline lines (Figure 2). It is likely that the partial crystalline structure was a result of lower than necessary cooling rates after the deposition.

Table 1. Chemical Composition of the Studied Alloys.

Alloy	Approximate Composition A – Weight %, B – Atomic %	Type of Alloy, Specimen
316 SS	70Fe-18Cr-10Ni-2.5Mo [A]	Polycrystalline, Disc
C-22	57Ni-22Cr-13Mo-3W-3Fe [A]	Polycrystalline, Disc and MCA
SAM2X5	49.7Fe-18.1Cr-15.2 B-7.4Mo-3.8C-2.4Si-1.9Mn-1.6W [B]	Amorphous coating

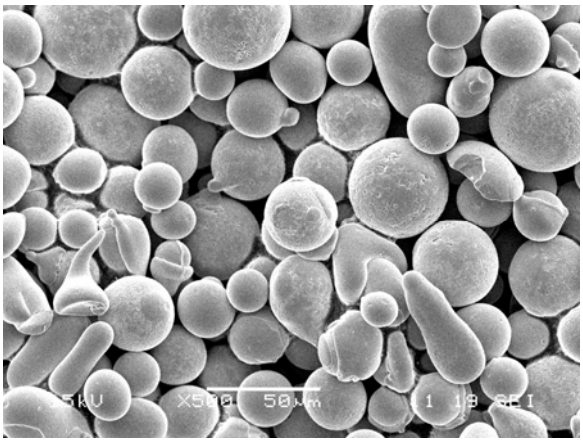

Figure 1. SEM image of SAM2X5, powder used for the coating of the MCA specimens

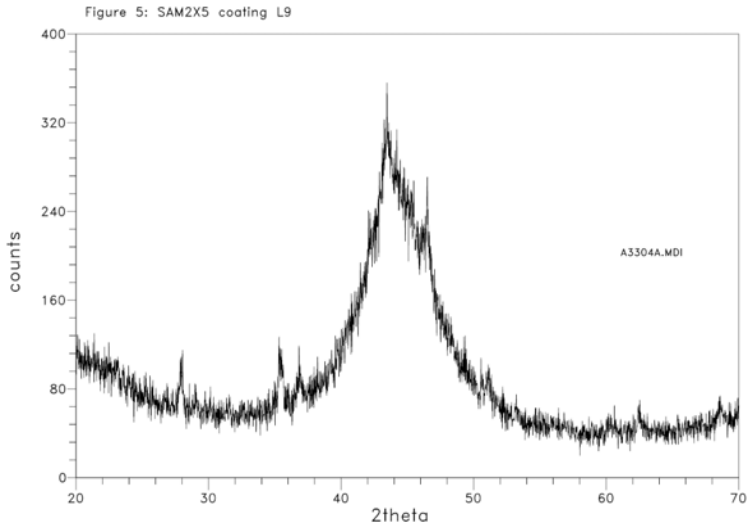

Figure 2. X-Ray diffraction pattern of SAM2X5 coated MCA electrochemical specimen

During the electrochemical testing at Lawrence Livermore National Laboratory, the SAM2X5 coated MCA was partially immersed in the test solution to provide a test area of 17.5 cm². The MCA specimens had two ceramic crevice formers attached on each side (Figure 3) to provide occluded regions to facilitate the formation of crevice corrosion. Before assembling onto the test specimens, the crevice formers were layered with a 0.003-inch thick PTFE tape to fill in the porous surface of the ceramic crevice formers and provide a tighter gap.

A three-electrode cell (ASTM G5) [14] (Figure 3), with a capacity of one liter, was used for all the experiments. Generally, 900 mL of electrolyte solution was used in each test. A saturated silver/silver chloride (Ag/AgCl, pre-filled with 4 M KCl saturated with AgCl) reference electrode was used for measuring the potential of the working electrode. The tests were conducted in a series of electrolyte solutions from pure sodium chloride to multi-ionic solutions such as saturated basic water (BSW) and natural seawater (from Half Moon Bay, CA). The

BSW solution is an alkaline concentrated version of the ground water at the Yucca Mountain site in Nevada. The electrochemical tests were conducted at 30°C and 90°C. Table 2 shows a list of the electrolyte solutions. A water cooled jacket was used to maintain the reference electrode at near room temperature. A platinum (Pt) sheet welded to a Pt wire was used as a counter electrode. The electrochemical cell was heated using a heating mantle. Nitrogen gas was bubbled through the test solution for deaeration. The gas exited the cell though a condenser and a liquid trap to prevent evaporation of the solution and the ingress of air into the test cell. The deaeration was started 24 hour before the electrochemical tests. During this period the evolution of the corrosion potential was monitored. The electrochemical polarization measurements were conducted through a Gamry commercial potentiostat that was integrated with a desktop computer and the companion software.

The electrochemical test sequence consisted of three steps; (1) Monitoring the corrosion potential for 24 h, (2) Three consecutive polarization resistance tests (ASTM G 59 and G 102) [14], and (3) A cyclic potentiodynamic polarization (CPP) (ASTM G 61) [14] test. For the polarization resistance and the CPP polarization tests, a potential scan rate of 600 mV per hour (0.167 mV/s) was used. In the polarization resistance tests the potential was scanned from 20 mV below the instantaneous corrosion potential to 20 mV above the corrosion potential. This test lasts approximately 4 minutes. For the CPP tests the scan was started at 20 mV below the instantaneous corrosion potential, and the scan was reversed when the current density reached 0.5 mA/cm² or 0.8 V. From the CPP tests several parameters can be obtained. These parameters are grouped into (1) Breakdown potentials (E20 and E200, which are the potentials in the forward scan that need to be reached to obtain current densities of 20 and 200 μA/cm² respectively) and (2) Repassivation potentials (ER10, ER1 and ERCO). ER10 and ER1 are the potentials in the reverse scan that need to be reached to obtain current densities of 10 and 1 μA/cm². ERCO is the potential at which the reverse scan crosses over (CO) the forward scan.

The corrosion rate was estimated from the polarization resistance tests using the following formulas given in ASTM standards G 59 and G 102 [14]

$$i_{corr} = \frac{1}{R_p} \times \frac{b_a \cdot b_c}{2.303\left(b_a + b_c\right)}$$

$$CR(\mu m / yr) = k \frac{i_{corr}}{\rho} EW$$

where k is a constant (3.27 x 10^{-3} mm g/μA cm yr). The Tafel constants b_a and b_c were assumed to be ± 120 mV/decade, the density (ρ) of all the amorphous alloys were taken as 8 g/cm³ and the equivalent weight (EW) as 26-dimensionless.

Results

Corrosion Potential and Corrosion Rate of Coated MCA Specimens

Table 2 shows the individual corrosion potential (E_{corr}) and the average corrosion rates at the end of the 24-hr immersion in the testing electrolyte solutions. The corrosion rate (CR) is the

average of three values measured on the same specimen. Both the E_{corr} and CR values in Table 2 are for a short immersion time in deaerated solutions and they are not intended to represent the values that this alloy may adopt for longer immersion time in naturally aerated solutions.

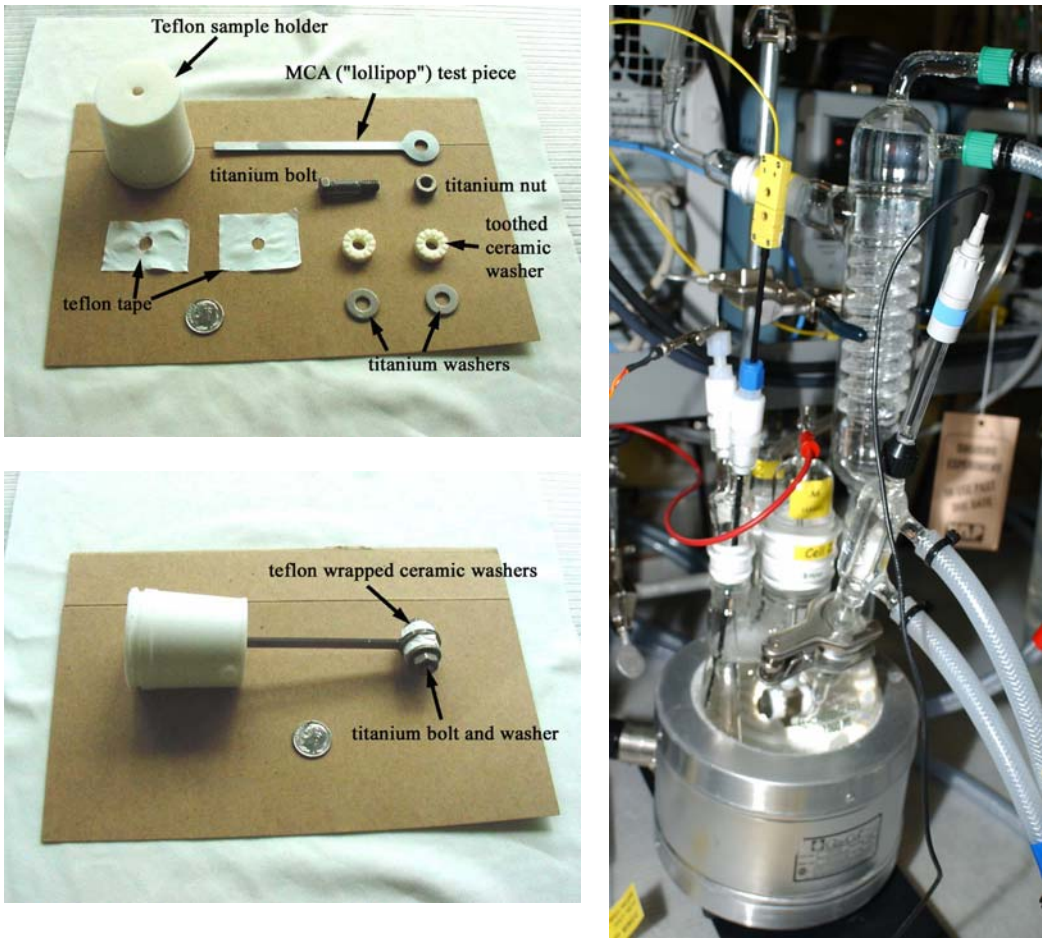

Figure 3. MCA-type specimens and testing cell

Figure 4 shows the evolution of the corrosion potential for the 24-hr immersion period for the coated specimens in 1 m NaCl solution (neutral and pH 2) both at 30°C and 90°C. For the neutral solutions, the corrosion potential decreased as time increased; first rapidly and after approximately 5-hr immersion, more slowly. At 90°C the corrosion potential was lower than at 30°C, showing that the alloy was more active at the higher temperature. For the pH 2 solution, there was little difference in the corrosion potential between 30°C and 90°C. For the pH 2 solutions the E_{corr} was higher than for the neutral solutions, as it could be predicted from the Pourbaix diagrams for iron and chromium.

Table 2 also shows that there was little difference in the E_{corr} of the SAM2X5 coated electrodes between 1 m NaCl and 3.5 m NaCl solutions at the same temperature and pH. Table 2 also shows little effect on the E_{corr} caused by addition of nitrate (NO_3^-) to the neutral chloride solutions, probably because nitrate does not become oxidizing until a lower pH is reached.

Table 2. Experimental Results using MCA or Lollipop Specimens Coated with SAM2X5 Amorphous Powder

Specimen	Solution	pH	Temp. (°C)	E_{corr} 24-hr.	Ave. CR (µm/year)	E20 mV SSC	E200 mV SSC	ER10 mV SSC	ER1 mV SSC	ERCO mV SSC
L9	1 m NaCl	NA	30	-542	10	-251	140	-231	-276	-193
L8		NA	90	-674	41	-502	-65	-313	-337	
L17	1 m NaCl	2	30	-338	84	-246	92	-223	-252	
L16		2	90	-336	2176	-335	-310	-249	-252	
L13	1 m NaCl + 0.15 m KNO3	NA	30	-520	9	-196	504	-175	-199	-154
L12		NA	90	-531	18	-349	-9	-221	-262	-91
L7	3.5 m NaCl	NA	30	-529	12	-236	476	-214	-271	
L6		NA	90	-448	33	-286	-107	-340	-359	-336
L15	3.5 m NaCl	2	30	-319	140	-274	110	-216	-242	
L14		2	90	-321	2852	-320	-306			
L11	3.5 m NaCl + 0.525 m KNO3	NA	30	-485	13	-193	151	-197	-217	-178
L10		NA	90	-527	22	-328	-95	-258	-293	-198
L3	Seawater	NA	30	-411	6	86	523	-201	-241	-221
L2		NA	90	-642	18	-408	-18	-335	-383	-159
L5	BSW	NA	30	-248	4	113	605	-156	-178	-178
L4		NA	90	-345	33	-191	-49	-193	-203	-181
316 Disc	Seawater	NA	90	-223	0.014	144	146	-91	-204	
C-22 Disc	Seawater	NA	90	-318	3.031	414	673	440	-122	852
C-22 MCA	Seawater	NA	90	-478	4.472	371	509	-6	-68	-49

m = concentration in molal (moles of solute per kg of solvent)
NA = Non-adjusted, as-prepared or neutral pH, BSW = basic saturated water

Figure 5 shows the average corrosion rate of the coated MCA electrodes as a function of the testing temperatures in 1 m NaCl and 3.5 m NaCl solutions, both neutral and pH 2. Both, for neutral and pH 2 solutions, the corrosion rate increased as the testing temperature increased; however, the increase was faster for the acidic solution. In the neutral solutions there was no difference in the corrosion rate between 1 m and 3.5 m NaCl solutions; however, in the pH 2 solution the corrosion rate in the 3.5 m NaCl solution was slightly higher than in the 1 m NaCl solution (Figure 5). The corrosion rates values in Figure 5 are for short-term immersion conditions in deaerated, simple salt electrolytes, and they are not intended to represent the behavior of this material in practical long-term industrial applications.

Table 2 shows that for all the tested electrolyte solutions the corrosion rate was higher at the higher temperature. However the increase in corrosion rate due to a temperature increase was not the same for all the tested solutions. This increase was as high as 25 times for the 1 m NaCl

pH 2 solution while it was only approximately 2 times higher in the NaCl + KNO_3 solutions (Table 2).

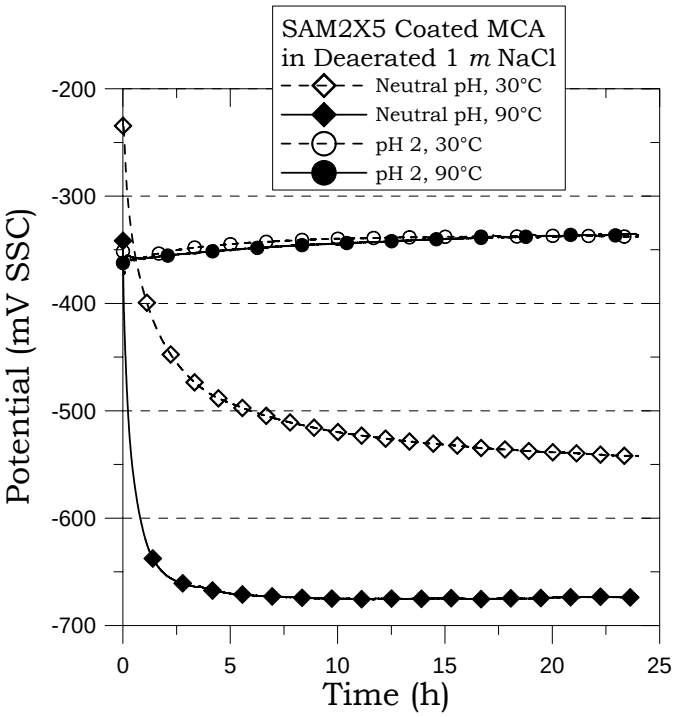

Figure 4. Corrosion potential as a function of immersion time

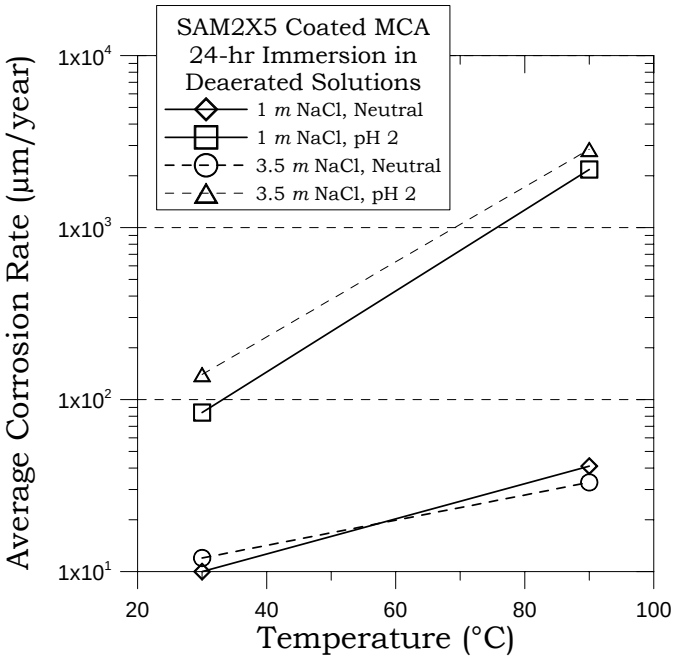

Figure 5. Corrosion rate as a function of testing temperature

Cyclic Potentiodynamic Polarization (CPP) studies

Figure 6 shows the cyclic potentiodynamic polarization (CPP) curves for the SAM2X5 coated material in neutral 1 m NaCl solution at 30°C and 90°C. As expected, as the temperature increased, the corrosion potential slightly decreased and the corrosion current and passive current density increased. The reverse scan curve shows a small hysteresis at 30°C and little or no hysteresis at 90°C. Both specimens were free from localized corrosion after the tests; however the exposed surfaces were yellow due to the anodic oxidation (Table 3). It is likely that the hysteresis observed in for the specimen tested at 30°C was the result of surface transformation (accumulation of a film consisting in mixtures of salts, oxides and hydroxides) due to the anodic applied potentials.

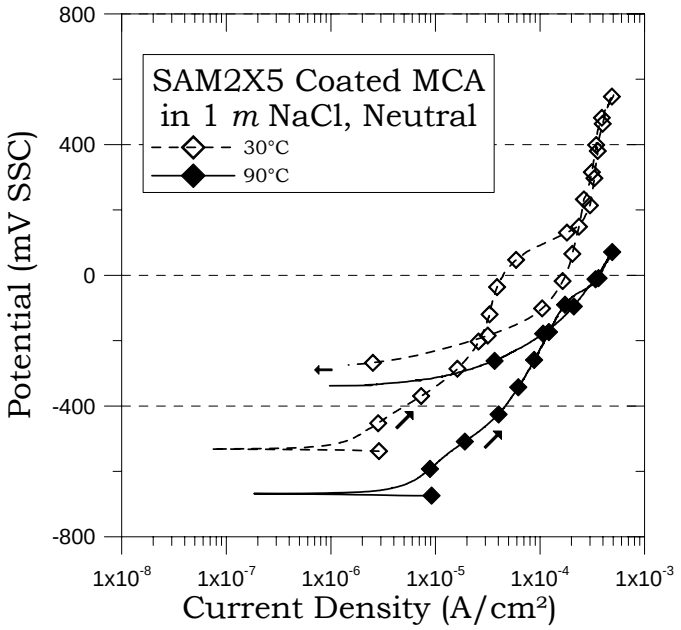

Figure 6. Cyclic potentiodynamic polarization(CPP) in 1 m NaCl at 30°C and 90°C

Table 2 shows the parameters obtained from the CPP tests. Both E20 and E200 represent values of breakdown potential and ER10, ER1 and ERCO represent values of repassivation potential. The higher the values of E20 and E200, the more resistant is the alloy to corrosion under anodic conditions. The higher the values of ER10, ER1 and ERCO, the higher the resistance of the alloy to localized corrosion. Table 2 shows that both the breakdown and the repassivation potentials for the coated electrodes are rather low, indicating that under the tested conditions, the coated SAM2X5 alloy was not highly resistant to corrosion. For example, of all the tested environments in Table 2, the highest ER1 value was only -178 mV SSC (in BSW solution at 30°C). The lowest resistance to anodic polarization was in seawater at 90°C where the ER1 was just -383 mV SSC.

In spite of the low resistance to corrosion of the coated specimens in the tested conditions, there was still a beneficial effect of nitrate on promoting passivation. Figure 7 shows the repassivation potential ER1 as a function of temperature for pure neutral NaCl solutions and for the same solutions with the addition of nitrate to a ratio of [NO3]/[Cl] of 0.15. Figure 7

shows that at both temperatures and for both base concentration of chloride, the presence of nitrate raised the value of ER1 by approximately 50 mV.

Table 3. Observations of the specimens after the CPP tests

Specimen	Solution	pH	Temp. (°C)	Observations
L9	1 m NaCl	NA	30	Yellow/brown surface, no crevice corrosion
L8		NA	90	Brown/tan surface, no crevice corrosion
L17	1 m NaCl	2	30	Light brown, no crevice corrosion
L16		2	90	Black staining, no crevice corrosion
L13	1 m NaCl + 0.15 m KNO3	NA	30	Pin point rusting, no crevice corrosion
L12		NA	90	Cracks on coating, light yellow, no crevice corrosion
L7	3.5 m NaCl	NA	30	Cracks on coating, rusting, no crevice corrosion
L6		NA	90	Black corrosion products, no crevice corrosion
L15	3.5 m NaCl	2	30	Light tan, no crevice corrosion
L14		2	90	Black corrosion products, no crevice corrosion
L11	3.5 m NaCl + 0.525 m KNO3	NA	30	Rusting, cracks on coating, no crevice corrosion
L10		NA	90	Light yellow, cracks on coating, no crevice corrosion
L3	Seawater	NA	30	Rusting, no crevice corrosion
L2		NA	90	Rusting, crack son coating, no crevice corrosion
L5	BSW	NA	30	Light tan, no crevice corrosion
L4		NA	90	Heavy rusting, probable pitting, no crevice corrosion

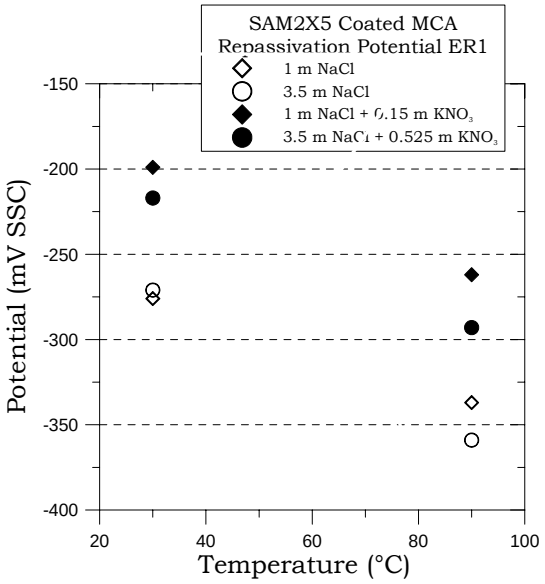

Figure 7.Effect of nitrate on the repassivation potential of SAM2X5 coated specimens

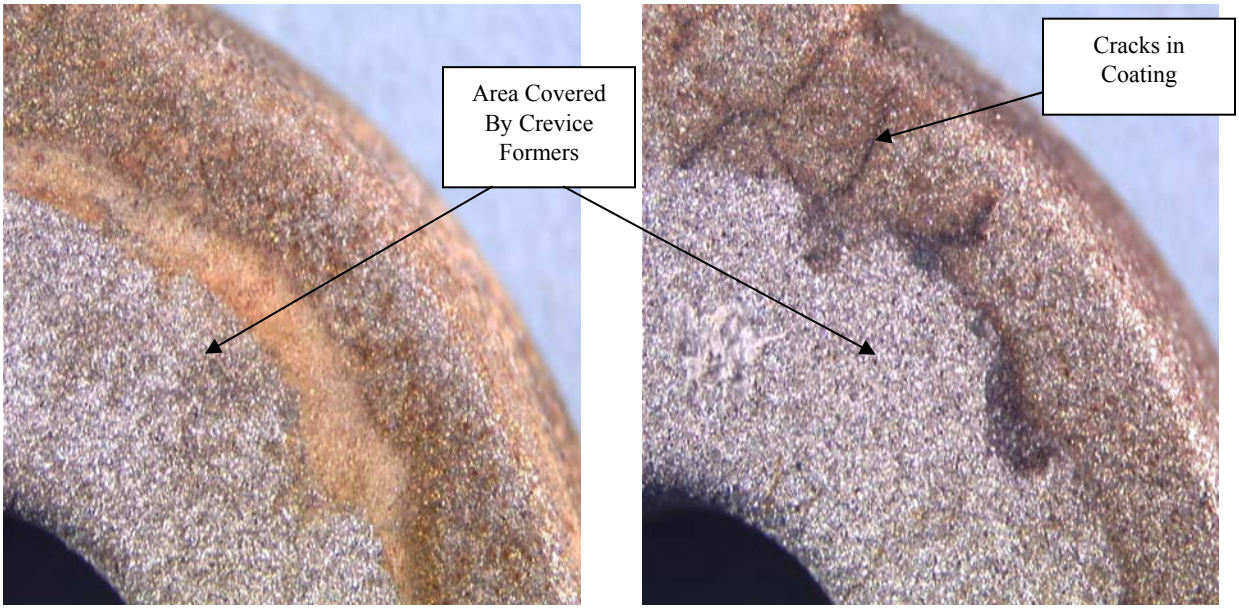

Specimen L3, Seawater, 30°C Specimen L2, Seawater, 90°C

Figure8. Appearance of the specimen after anodic polarization in seawater

Figure 8 shows the appearance of two specimens after the CPP test in seawater. None of the specimens suffered crevice corrosion (Table 3). It is likely that the high rugosity of the coating avoided the formation of a tight gap between the crevice former and the specimen and consequently crevice corrosion did not occur. The specimen tested at 30°C (L3) was polarized to higher potentials than the specimen tested at 90°C (L2) (Table 2); therefore the color appearance is different (Figure 8). Specimen L2 appeared to have suffered cracking in the coating. It is not known if the coating was cracked before the test or if cracking occurred as a consequence of the electrochemical testing.

Comparative Polarization (CPP) studies

Figure 9 shows the comparative CPP curves for the SAM2X5 coated material and other alloys of relevance. Figure 9 shows that the lowest resistance to corrosion for all the materials was for the coated material. The highest resistance was for the SAM2X5 ribbon. One of the reasons that the SAM2X5 coated MCA did not perform satisfactorily could be because of the partial crystalline structure of the coating (Figure 2).

The industrial use of amorphous coatings is not only for corrosion protection but also as a vehicle for boron, a desirable element for neutron absorption applications [10-11]. Therefore the current results on coated electrochemical specimens showing low resistance to corrosion are not disappointing news for the application of these coatings. For neutron absorption applications, the environments of interest are not as aggressive as the ones used in the current test matrix.

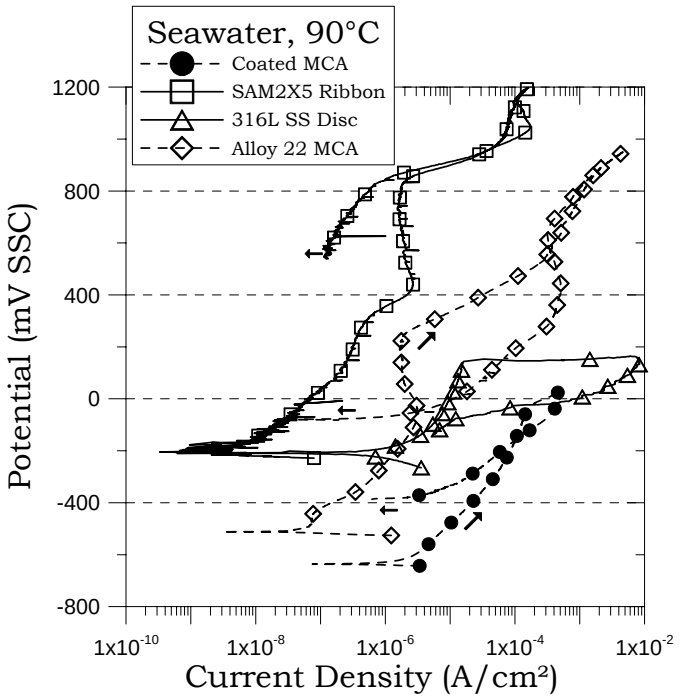

Figure 9. Comparative polarization studies between the SAM2X5 coated MCA and other materials

Summary and Conclusions

- Iron-based amorphous coatings of SAM2X5 were tested electrochemically in several solutions both at 30°C and 90°C.
- At the open circuit potential, the general corrosion rate was low, except for the pH 2 solutions.
- Under anodic polarization, the coatings did not suffer crevice corrosion maybe because a tight gap could not be formed between the rugose coating and the applied crevice former.
- Under anodic polarization, the coated materials were less resistant to corrosion than amorphous ribbons prepared using high solidification rates.

Acknowledgements

This work was performed under the auspices of the U. S. Department of Energy by the University of California Lawrence Livermore National Laboratory under contract W-7405-Eng-48. Work was sponsored by the United States Department of Energy (DOE), Office of Civilian Radioactive Waste Management (OCRWM) and the Defense Advanced Research Projects Agency (DARPA), Defense Science Office (DSO). The guidance of Leo Christodoulou at DARPA DSO and of Jeffrey Walker at DOE OCRWM is gratefully acknowledged.

Disclaimer

References

1. J. R. Scully and A. Lucente, "Corrosion of Amorphous Metals," ASM Handbook, Volume 13B, Corrosion: Materials, p. 476 (ASM International, 2005: Materials Park, OH).
2. K. Hashimoto, K. Asami, M. Naka and T. Masumoto, Corr. Sci., 19, 857 (1979)
3. K. Asami, M. Naka, K. Hashimoto and T. Masumoto, J. Electrochem. Soc., 127, 76 (1991).
4. H. Habazaki, A. Kawashima, K. Asami and K. Hashimoto, J. Electrochem. Soc., 138, 2130 (1980).
5. R. B. Rebak, L. F. Aprigliano, S. D. Day, and J. C. Farmer, "Salt Fog Testing of Iron-Based Amorphous Alloys," Paper NN3.14, in proceedings of the symposium Scientific Basis for Nuclear Waste Management XXX in the Materials Research Society annual conference, 28 November to 01 December 2006, Boston MA.
6. J. R. Scully, A. Gebert and J. H. Payer, *Journal of Materials Research*, **22**, 302 (2007).
7. J. C. Farmer, J. J. Haslam, S. D. Day, D. J. Branagan, C. A. Blue, J. D. K. Rivard, L. F. Aprigliano, N. Yang, J. H. Perepezko and M. B. Beardsley, "Corrosion Characterization of Iron-Based High-Performance Amorphous-Metal Thermal-Spray Coatings," in proceedings of 2005 ASME PVP Conference 17-21 July 2005, Vol. 7, Operations, Applications and Components, p. 583 (New York, NY: ASME, 2005).
8. J. Shen, Q. Chen, J. Sun, H. Fan and G. Wang, Applied Physics Letters, 86, 151907 (2005).
9. L. Kaufman, J. H. Perepezko, and K. Hildal "Synthesis and Performance of Fe-Based Amorphous Alloys for Nuclear Waste Repository Applications," in proceedings of the Joint International Topical Meeting on Mathematics and Computation and Supercomputing in Nuclear Applications (M&C + SNA), organized by the American Nuclear Society in Monterey, CA 15-19 April 2007.

10. T. Lian, S. D. Day, P. D. Hailey, J. S. Choi and J. C. Farmer, "Comparative Study on the Corrosion Resistance of Fe-Based Amorphous Metal, Borated Stainless Steel and Ni-Cr—Mo-Gd Alloy," Paper NN8.7 in proceedings of the symposium Scientific Basis for Nuclear Waste Management XXX in the Materials Research Society annual conference, 28 November to 01 December 2006, Boston MA.

11. J. C. Farmer "Corrosion-Resistant Iron-Based Amorphous-Metal Coatings," Paper PVP2006-ICPVT11-93421 in the 2006 Pressure Vessels & Piping Conference and the Eleventh International Conference on Pressure Vessel Technology, 23-27 July 2006, Vancouver, BC, Canada.

12. ASTM B932–04 "Standard Specification for Low-Carbon Nickel-Chromium-Molybdenum-Gadolinium Alloy Plate, Sheet, and Strip," (ASTM International, 2004: West Conshohocken, PA).

13. T. E. Lister, R. E. Mizia, P. J. Pinhero, T. L. Trowbridge, and K. Delezene-Briggs, "Studies of the Corrosion Properties of Ni-Cr-Mo-Gd Neutron-Absorbing Alloys," *Corrosion*, **61**, 7, 706, 2005.

14. ASTM International, Volume 03.02, Corrosion of Metals, (ASTM International, 2004: West Conshohocken, PA).